

Modelling of Mass Transfer in Gas-Liquid Stirred Tanks Agitated by Rushton Turbine and CD-6 Impeller

J. Gimburn, C. D. Rielly*, Z. K. Nagy

Dept. Chemical Engineering, Loughborough University, Leics, LE11 3TU, UK.
e-mail: c.d.rielly@lboro.ac.uk

Abstract. A combined computational fluid dynamics (CFD) and population balance model (PBM) approach has been applied to simulate gas-liquid stirred tanks agitated by (i) a Rushton turbine and (ii) a CD-6 impeller, operating at aeration numbers from 0.017 to 0.038. The multiphase simulations were realised via an Eulerian-Eulerian two-fluid model and the drag coefficient of spherical and distorted bubbles was modelled using the Ishii-Zuber equations. The effect of void fraction on the drag coefficient was modelled using the correlation by Behzadi *et al.* The local bubble size distribution was obtained by solving the PBM using the quadrature method of moments (QMOM). The local $k_L a$ was estimated using both the Higbie penetration theory and the surface renewal model. The predicted gas-liquid hydrodynamics and local bubble sizes were in good agreement with experimental measurements reported in the literature. An improvement on the prediction of the aerated power number was obtained using the non-uniform bubble size distribution resulting from the coupled CFD-PBM simulation. The results show that the CD-6 impeller provides much better gas dispersion and mass transfer coefficients compared to the Rushton turbine. It was observed that the gas dispersion in a larger scale tank was more inhomogeneous and has a lower $k_L a$ in comparison to the smaller tanks, in which a larger volume of dead zone was present. Considering its predictive capability, the method outlined in this work can provide a useful scale-up evaluation of gas-liquid stirred tanks.

Key words: gas-liquid; mass transfer; local bubble size; QMOM; CD-6; scale-up; CFD-PBM

1. INTRODUCTION

There are many industrial processes that involve gas-liquid dispersion in stirred tanks, *e.g.* in fine-chemical manufacturing, or in biochemical fermentations. For economic and safety reasons, reliable models are needed for the scale-up and design of such reactors. One of the most important problems in modelling gas-liquid dispersions is the prediction of bubble size and gas-liquid interfacial area. As shown experimentally by many researchers (*e.g.* Barigou and Greaves [1]; Laakkonen *et al.* [2, 3]) the distribution of bubble sizes varies inside the stirred tank depending on the spatial position. Generally, bubble sizes around the impeller discharge stream are the smallest due to breakage caused by the high turbulence dissipation rates. Knowledge of bubble sizes is necessary in a two-phase CFD model to calculate momentum exchange by drag. Hence, the population balance, phase continuity and momentum equations are coupled and should be solved together. In addition, local bubble sizes and the local gas volume fraction are required for the calculation of the interfacial area, which is an important variable in designing an aerated stirred tank to achieve a required rate of gas-liquid mass transfer.

The first part of this work focuses on the development of a modelling approach for multiphase stirred tanks. For an initial comparison, the CFD simulation was performed assuming a constant bubble size throughout the tank. A coupled CFD-PBM simulation was then performed to account for the spatially non-uniform bubble sizes inside the tank. The CFD prediction of the two-phase flow field was compared to experiments by Deen and Hjertager [4], whereas the results using the CFD-PBM approach were compared against measurements by Laakkonen *et al.* [3]. After validation, the model was used to evaluate the local mass transfer coefficients inside the tank, and to evaluate the reactor scale-up, especially from the mass transfer perspective, which is often vital in aerobic fermentation.

2. MODELLING APPROACH

The 14L and 200L aerated stirred tanks containing a Rushton turbine, studied by Laakkonen *et al.* [3] were considered for the CFD-PBM modelling. Gas was injected through a sparger ring at a flow rate ranging from 0.29 to 0.7 vvm. First, a two-phase CFD simulation was performed assuming a uniform bubble diameter throughout the tank. The interphase drag coefficient was estimated using the standard Schiller-Naumann drag model. The CFD simulation was performed using a half-tank domain consisting of about 225k hexahedral cells. The impeller movement was modelled using a multiple reference frame and the Eulerian-Eulerian approach was employed for the multiphase modelling. The turbulence was modelled using the two-phase realizable $k-\varepsilon$ model. Transient solvers with second-order implicit time advancement and the third-order (QUICK) spatial interpolation scheme were also applied. The iteration residual was set to fall below 1×10^{-4} at each time step to achieve good convergence. The volume average of the gas void fraction at the rotating zone (impeller region) was also monitored and the iterations were only halted once a constant value was observed. A grid sensitivity study was performed prior to the final grid selection using three different meshes: coarse (165k), intermediate (225k) and fine (335k). It was found that the domain consisting of 225k cells yielded a grid independent solution.

The QMOM was employed to solve the population balance equation. The evolutions of the abscissas and weights were calculated using the product difference (PD) algorithm of Gordon [5]. The bubble breakage and coalescence kernels were from the Prince and Blanch [6] model. The population balance model was solved as a user-defined scalar implemented via user-defined subroutine written in C. The user-defined subroutine is compiled within the commercial CFD code, FLUENT 6.3 and is available as an add-on program after the compilation; hence a coupled CFD-PBM simulation can be performed. Bubbles have a tendency to form a non-spherical shapes for diameters greater than about 3 mm. Therefore, the drag model of Ishii and Zuber [7] was selected since it takes into account the drag of distorted bubbles. The effect of the void fraction of bubbles on the drag was accounted for using the correlation by Behzadi *et al.* [8].

Having obtained the local bubble size, the local $k_L a$ was then estimated using two common methods, namely Higbie's [9] penetration theory and the surface renewal method [10]. Once the local $k_L a$ values had been obtained, the oxygen transfer rate in the tank was estimated: the transport equation for dissolved oxygen mass fraction was also solved as a user-defined scalar implemented as a user-defined subroutine.

3. RESULTS AND DISCUSSION

3.1 Prediction of Gas-Liquid Hydrodynamics

First, the CFD simulations were validated against experimental data using the two-phase PIV measurements reported by Deen and Hjertager [4] on a stirred tank with $Fl_g = Q_g/ND^3 =$

0.0296. The impeller speed for Laakkonen's geometry was set to 513 rpm to ensure the aeration number stayed at $Fl_g = 0.0296$ so that a sensible comparison between the CFD prediction and the experimental measurement from Deen and Hjertager [4] could be made.

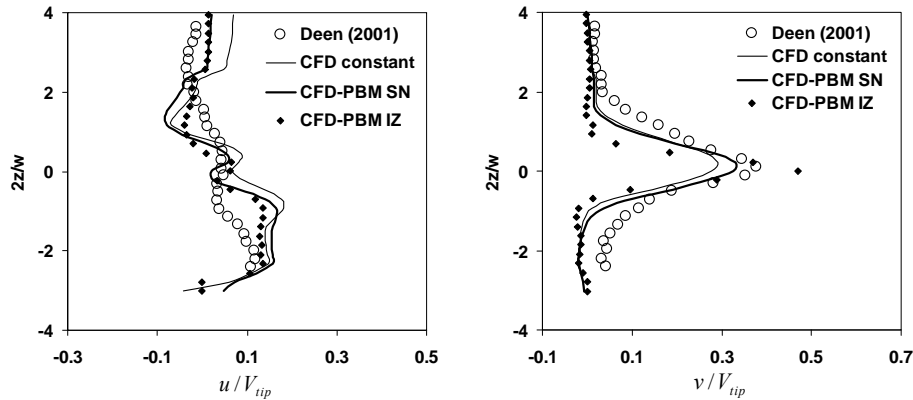


Fig. 1: Prediction of gas phase axial (u) and radial (v) velocity at normalised radial position (radial position, r over tank radius, R) $r/R = 0.37$. Schiller-Naumann [11] drag model (CFD-PBM-SN), Ishii-Zuber [7] drag model (CFD-PBM-IZ). Experimental data from Deen and Hjertager [4].

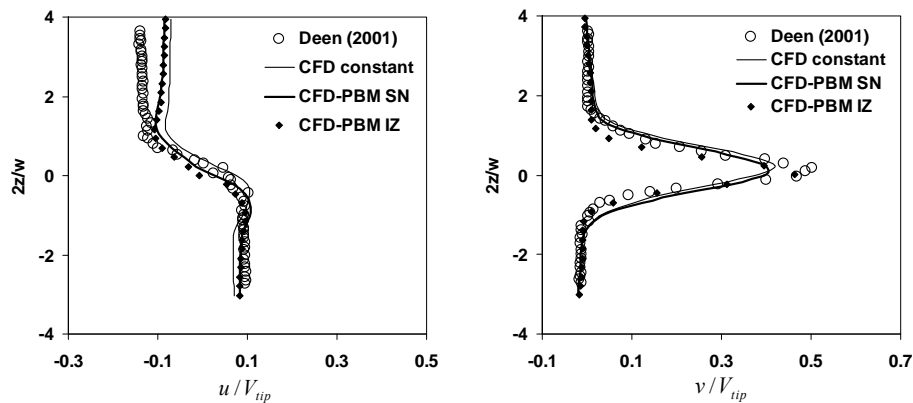


Fig. 2: Prediction of liquid phase axial and radial velocity at $r/R = 0.37$. Experimental data from Deen and Hjertager [4].

The simulation was performed initially by assuming a constant bubble size of 3.5 mm throughout the tank. The bubbles were assumed to be spherical and the Schiller-Naumann [11] drag model was employed to estimate the drag coefficient. The CFD result was time-averaged over all blade angles and compared with Deen and Hjertager's [4] PIV measurements. For easier comparison, the results for the mean velocities were normalised using the impeller tip velocity (V_{tip}). Despite the assumption of a constant bubble size and spherical bubbles, the predictions (marked as CFD constant) shown in Figs. 1 and 2 are reasonably close to the experimental data. The differences can be explained by the bubble coalescence and break-up caused by the turbulent flow induced by the rotating impeller. These mechanisms are not considered in the case where a constant bubble size is assumed throughout the tank.

A simulation using a non-uniform bubble size was next performed to evaluate this effect on the CFD predictions. The local bubble sizes were estimated using the population balance model, which tracks the moments of the bubble size distribution. The local Sauter mean diameters (d_{32}), obtained from the ratio of third and second moments, were then passed into

the CFD simulation and used for the two-phase flow modelling. The CFD-PBM simulations were performed using two different drag models, a spherical drag model [11] and another that takes into account the drag of distorted bubbles [7]. As expected, results obtained from the CFD-PBM modelling were better compared to those obtained using a constant bubble size. The prediction of axial *gas* velocities below the impeller ($2z/w < 1$) and the peak liquid radial velocities were in better agreement with Deen's [4] data. Using the non-spherical drag model (CFD-PBM-IZ) in the CFD-PBM approach further improved the results. This is due to the fact that the effect of local bubble sizes on the two-phase flow is mainly via the interphase exchange coefficient, which depends on the drag model. The Schiller-Naumann model is suitable for spherical rigid bubbles, but in comparison, the Ishii-Zuber model predicts drag coefficients for the spherical, ellipse and cap bubble regime. The difference observed between the flow field predicted using a spherical drag model and the one that accounts for distorted bubbles is negligible for the cases considered in this paper, due to the proximity of the analysed region to the impeller tip. In this region, the bubble size is mainly below 3 mm and hence bubbles can be assumed to be approximately spherical. Because of the better prediction of the gas-liquid flow mean velocities, the CFD-PBM-IZ was selected and used for the remainder of this work. The remaining discrepancy in the result predicted by CFD-PBM-IZ method might be due to minor differences in the tank geometry used by Deen and Hjertager [4] and Laakkonen *et al.* [3] (this work).

3.1 Prediction of the Aerated Power Number

Prediction of the gassed power input by integrating the dissipation rate (ϵ) over the tank volume is known to provide an underestimate of the power input, therefore the P_g in this work was calculated from the moment acting on the shaft and impeller or baffles and tank wall. The calculated torque, T , is then related to the power input by,

$$P_g = 2\pi NT \quad (1)$$

For a Rushton turbine Bujalski *et al.* [12] suggested the following correlation for estimation of the ungassed power number:

$$N_{p0} = \frac{P_0}{\rho_l N^3 D^5} = 2.512 \left(\frac{t}{D} \right)^{-0.195} T^{0.063} \quad (2)$$

where t is the impeller thickness and T is the tank diameter (m). Smith [13] proposed the following correlation for the relative power draw, P_g/P_0 , for stirred tanks agitated by a Rushton turbine, based on the measurements of Warmoeskerken and Smith [14] and Gezork *et al.* [15]:

$$P_g/P_0 = 0.18 Fr^{-0.2} Fl_g^{-0.25}, \quad (3)$$

where Fr and Fl_g are the Froude number and the aeration number, respectively. Myers *et al.* [16] performed extensive experiments in single phase and aerated stirred tank with a CD-6 impeller; they reported that the P_g/P_0 of a Rushton turbine drops significantly compared to that of a CD-6 impeller. In this study the CFD predictions were compared with measured P_g/P_0 obtained from Myers *et al.* [16] for CD-6 impeller, and using eq.(3) for the Rushton turbine, together with eq.(2).

The P_g/P_0 is shown to be predicted reasonably well using the assumption of a constant bubble sizes throughout the tank (see Table 1). There is a small improvement in the prediction of P_g/P_0 when a non-uniform bubble size is employed using the CFD-PBM method, especially for cases 1, 4, 5 and 6 for which the bubble sizes used for the initial simulation differed significantly from those calculated using the PBM. The bubble sizes for cases 2 and 3 are known from Laakkonen *et al.* [3], and were used for the initial CFD simulation. Consequently, the CFD predictions using uniform bubble sizes for cases 2 and 3 are much

closer to the values estimated from eq.(3). The results suggest that the P_g/P_0 can be predicted reasonably well using the uniform bubble size assumption with bubble size close to the experimental mean values. However, the CFD-PBM method is a more suitable approach for predicting the relative power number in the case when the bubble size is not known.

Table 1: Prediction of the relative power number for Rushton Turbine (RDT)

Case	T (m)	D (m)	F_{lg}	vvm	v_g (cm/s)	N (rpm)	\bar{d}_{32} (mm)	Relative power number		
								P_g/P_0 eq.(3)	P_g/P_0 CFD constant d_b	P_g/P_0 CFD-PBM-IZ
1	0.26	0.086	0.030	0.70	0.30	513.0	2.7	0.47	0.44	0.48
2	0.26	0.086	0.022	0.70	0.30	700.0	2.4	0.45	0.41	0.47
3	0.63	0.210	0.038	0.70	0.74	390.0	3.5	0.42	0.38	0.43
4	0.63	0.210	0.022	0.37	0.39	365.8	4.0	0.49	0.43	0.50
5	0.63	0.210	0.038	0.70	0.74	386.4	4.3	0.42	0.39	0.44
6	0.63	0.210	0.017	0.29	0.30	357.6	3.9	0.53	0.42	0.51

Table 2: Prediction of the relative power number for CD-6

Case	T (m)	D (m)	F_{lg}	vvm	N (rpm)	\bar{d}_{32} (mm)	Relative power number		
							P_g/P_0 measured [16]	P_g/P_0 CFD constant d_b	P_g/P_0 CFD-PBM-IZ
7	0.26	0.086	0.22	0.70	698	3.2	0.71	0.75	0.73

3.2 Prediction of Local Bubble Size and Mass Transfer Coefficient

CFD-PBM simulations were performed using a user-defined subroutine compiled within FLUENT. The Prince and Blanch [6] breakage and coalescence kernels were employed to predict the bubble dynamics throughout the tank. The volume-average Sauter mean diameter, d_{32} , in the impeller region was used as a convergence indicator in these simulations.

Figures 3 and 4 show that the local bubble sizes predicted by the CFD-PBM simulation for both the smaller and the larger tanks are predicted well and are in good agreement with the experiments by Laakkonen *et al.* [3]. The smallest bubbles can be observed around the impeller, where the dissipation rates are a maximum, whereas the largest bubbles are found below the impeller, just above the sparger, due to a combination of a high void fraction and low dissipation rates. Some discrepancies in the local bubble size predictions can be observed, possibly due to the well-known under-prediction of turbulence dissipation rate by the $k-\epsilon$ model. The evolution of the bubble size depends mainly on the dissipation rates and the gas void fraction. The CFD-PBM approach is also capable of responding to changes in operating conditions. For instance, case 1, which considers a lower impeller speed, produces much larger bubbles compared to case 2, where the impeller speed is much higher (see Table 1).

Using the local bubble size, the local k_{La} can be estimated using Higbie's [9] penetration theory and the surface renewal model [10]. Overall both methods gave similar k_{La} predictions, except around the impeller region where Higbie's method gave a significantly higher value (see Fig. 5). The local k_{La} values for the larger tank were significantly smaller than for the smaller tank. The local k_{La} contour map also revealed a large dead zone on the bottom region of the tank due to the poor gas dispersion produced by the Rushton turbine. This can be addressed by employing a better gas dispersion impeller such as the CD-6, as shown in Fig. 6A. The CD-6 impeller is a concave type impeller which is available commercially from Chemineer and has been studied extensively by many researchers (e.g. Myers *et al.* [16]). There are several reasons why the CD-6 disperses bubbles much better than the Rushton turbine. Firstly, the CD-6 pumps the fluid slightly downward around the impeller discharge

region, whereas the Rushton turbine pumps slightly upward (see Fig. 6A), which then contributes to poor circulation of bubbles in the lower region. Secondly, the concave shape of the CD-6 is designed to produce a smaller gas cavity behind the impeller blade (see Fig. 6B) leading to a reduction in the aerated power number in comparison to the Rushton turbine. The larger gas cavity means more coalescence hence poorer gas dispersion and a larger decrease in the gassed power input.

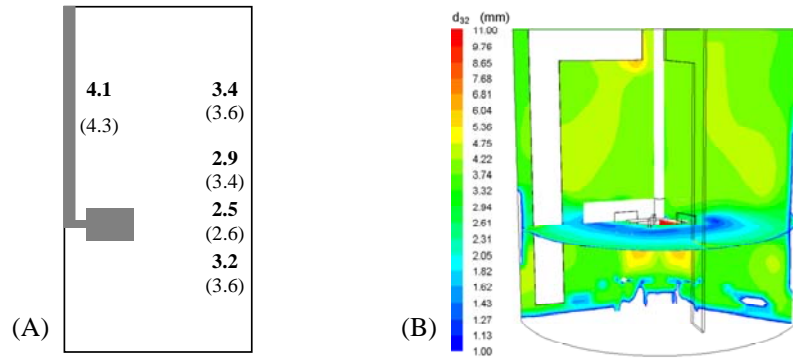


Fig. 3: Prediction of local Sauter mean bubble diameter for case 4: RDT, 200 L tank, $N = 390$ rpm, $Q_g = 0.7$ vvm. A) Laakkonen *et al.* [3] measurement (bold), this work (bracket), B) Contour map of Sauter mean diameter

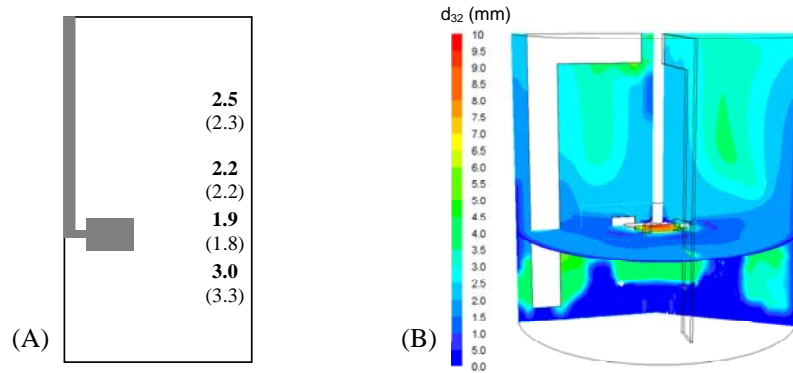


Fig. 4: Prediction of local Sauter mean bubble diameter for case 2: RDT, 14 L tank, $N = 700$ rpm, $Q_g = 0.7$ vvm. A) Laakkonen *et al.* [3] measurement (bold), this work (bracket), B) Contour map of Sauter mean diameter

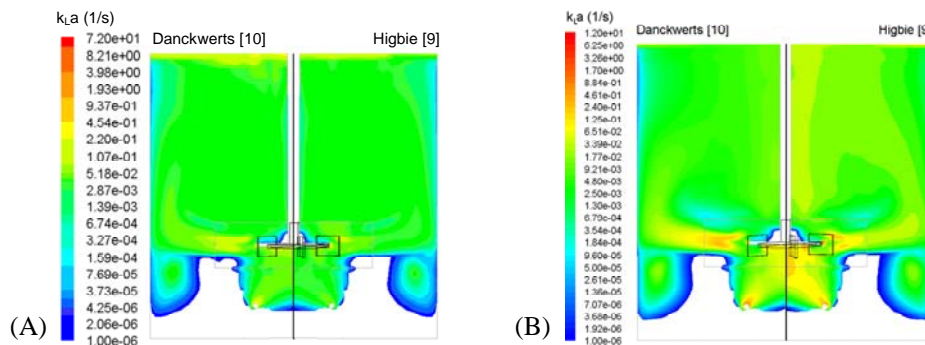


Fig. 5: Prediction of local $k_L a$ with a RDT. A) 14 L tank (case 2), B) 200 L tank (case 3)

By analogy with experimental measurements a global mean $\langle k_L a \rangle$ was estimated by monitoring the volume-averaged oxygen concentration, $C(t)$, throughout the simulation, from:

$$\ln\left(\frac{C^* - C(t)}{C^* - C_0}\right) = -\langle k_L a \rangle t \quad (4)$$

where C^* is the oxygen solubility in water and $C(t)$ is the oxygen concentration in the tank at time t . The volume averaged local values of $k_L a$ from CFD for case 3 were 0.009 and 0.012 for the Higbie and Danckwerts method's respectively. The values of $\langle k_L a \rangle$ obtained using eq.(4) were obtained from the slopes of the graphs obtained by plotting the left ahnd side of eq.(4) against time, as shown in Fig. 7A. The $\langle k_L a \rangle$ values obtained were similar at around 0.01 s^{-1} , for both the Higbie and Danckwerts methods, respectively. In eq.(4), and often in experimental measurements of the mass transfer coefficient, it is assumed that the dissolved oxygen concentration, [DO] is uniform. This well-mixed assumption is less likely to be correct with increasing scale [17]. Thus in practice, the [DO] may be non-uniform, being almost saturated in some locations where there is a high local $k_L a$, and having a low [DO] in regions with poor gas dispersion (see Fig. 7B). Hence there are differences between the results reported above. It may be concluded that simple volume averages of $k_L a$ from CFD simulations, without knowledge of their correlation with local driving forces, are of little practical use; they would tend to be larger than the global $k_L a$ values obtained by experiment, or from eq.(4). However, a CFD calculation which solves the oxygen transport equation, coupled with local values of $k_L a$ takes this effect into account, and can serve as a more correct framework for the design and scale-up of aerated stirred tanks than methods that use eq.(4) with volume averaged quantities.

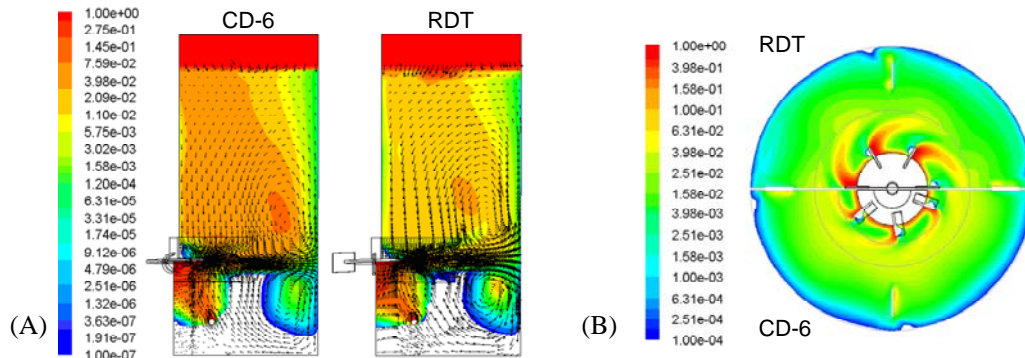


Fig. 6: Comparison of CFD-PBM-IZ prediction of the two-phase flow in the 14 L tank with a CD-6 impeller (case 7) and RDT (case 2): $P_g/V = 1174.7 \text{ W/m}^3$, $Q_g = 0.7 \text{ vvm}$, A) Velocity vectors; contours of gas void fraction, B) Contour of gas void fraction at the impeller level

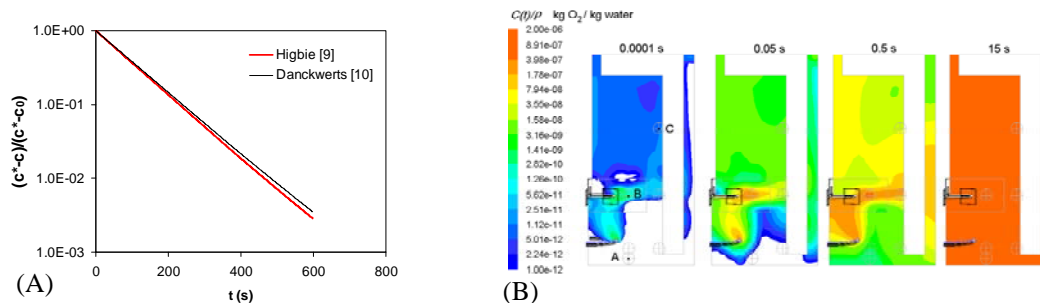


Fig. 7: Evolution of oxygen concentration in the 200 L tank, with a RDT: $N = 390 \text{ rpm}$, $Q_g = 0.7 \text{ vvm}$ (case 3), A) Volume averaged oxygen concentration, B) Contour map of local oxygen concentration

4. CONCLUSION

A comprehensive method via CFD-PBM for modelling aerated stirred tanks has been developed. The CFD-PBM method with a drag model suitable for spherical and distorted bubbles is shown to be a better approach for modelling the gas-liquid flows in stirred tanks. The power number, local bubble sizes and the mean velocities of the two-phase flow have been predicted satisfactorily in correspondence with experimental data taken from the literature. The scale-up of gas-liquid stirred tanks is a very challenging task because it is very difficult to maintain a similar mass transfer level from a small vessel to the bigger vessels. The results from these CFD-PBM predictions will be exploited further to investigate scale-up rules for gas-liquid stirred tank operations.

5. ACKNOWLEDGEMENT

JG acknowledges a scholarship from Ministry of Higher Education, Malaysia, and Universiti Malaysia Pahang. We also wish to thank Dr. D. L. Marchisio for sharing the single phase QMOM UDF which led to the implementation of multiphase QMOM UDF in this work.

6. REFERENCES

1. Barigou M., Greaves M., 1992. "Bubble-size distributions in a mechanically agitated gas-liquid contactor", *Chem. Eng. Sci.*, **47**, 2009-2025.
2. Laakkonen M., Moilanen P., Miettinen T., Saari K., Honkanen M., Saarenrinne P., Aittamaa J., 2005. "Local bubble size distributions in agitated vessel comparison of three experimental techniques", *Chem. Eng. Res. Des.*, **83**, 50-58.
3. Laakkonen M., Moilanen P., Alopaeus V., Aittamaa J., 2007. "Modelling local bubble size distributions in agitated vessels", *Chem. Eng. Sci.*, **62**, 721-740.
4. Deen N.G. and Hjertager B.H., 2002. "Flow generated by an aerated Rushton impeller: two-phase PIV experiments and numerical simulations", *Can. J. Chem. Eng.*, **80**, 638-652.
5. Gordon R.G., 1968. "Error bounds in equilibrium statistical mechanics", *J. Math. Phys.*, **9**, 655-663.
6. Prince M.J., Blanch H.W., 1990. "Bubble coalescence and break-up in air-sparged bubble columns", *AIChE J.*, **36**, 1485-1499.
7. Ishii M., Zuber N., 1979. "Drag coefficient and relative velocity in bubbly, droplet or particulate flows", *AIChE J.*, **25**, 843-855.
8. Behzadi A., Issa R.I., Rusche H., 2004. "Modelling of dispersed bubble and droplet flow at high phase fractions", *Chem. Eng. Sci.*, **59**, 759-770.
9. Higbie R., 1935. "The rate of absorption of a pure gas into a still liquid during short periods of exposure", *Trans. Am. Inst. Chem. Engrs.* **31**, 364-389.
10. Danckwerts P.V., 1951. "Significance of liquid-film coefficients in gas absorption", *Ind. Eng. Chem.* **43**, 1460-1467.
11. Schiller, L., Naumann, Z., 1935. "A drag coefficient correlation", *Z. Ver. Deutsch. Ing.*, **77**, 318.
12. Bujalski W., Nienow A.W., Chatwin S., Cooke M., 1987. "Dependency on scale of power numbers of rushton disc turbines", *Chem. Eng. Sci.*, **42**, 317-326.
13. Smith JM, 2006. "Large multiphase reactors some open questions", *Chem. Eng. Res. Des.*, **84(A4)**, 265-271.
14. Warmoeskerken M.M.C.G., Smith J.M., 1982. "Description of the power curves of turbine stirred gas dispersions", *Proc Fourth Europ Conf on Mixing*, Noordwijkerhout, BHRA, Cranfield, pp. 237-246.
15. Gezork K.M., Bujalski W., Cooke M., Nienow, A.W., 2000. "The transition from homogeneous to heterogeneous flow in a gassed stirred vessel", *Chem. Eng. Res. Des.*, **78A**, 363-370.
16. Myers K.J., Thomas A.J., Bakker A., Reeder M.F., 1999. "Performance of a gas dispersion impeller with vertically asymmetric blades", *Chem. Eng. Res. Des.*, **77**, 728-730.
17. Schuetze J., Hengstler J., 2006. "Assessing aerated bioreactor performance using CFD", 12th *European Conference on Mixing*, Bologna, June 27-30, 439-446.